

Nanomechanical Properties and Deformation Mechanism in Metals, Oxides and Alloys

Elias P. Koumoulos, Dimitrios A. Dragatogiannis
and Constantinos A. Charitidis

Abstract Metals, oxides and alloys are widely used in transport and industry-engineering applications, due to their functionality. In this work, the nanomechanical properties (namely hardness and elastic modulus) and nanoscale deformation of metals, oxides and alloys (elastic and plastic deformation at certain applied loads) are investigated, together with pile-up/sink-in deformation mechanism analysis, subjected to identical condition parameters, by a combined Nanoindenter—Scanning Probe Microscope system. The study of discrete events including the onset of dislocation plasticity is recorded during the nanoindentation test (extraction of high-resolution load–displacement data). A yield-type pop-in occurs upon low applied load representing the start of phase transformation, monitored through a gradual slope change in the load–displacement curve. The ratio of surface hardness to hardness in bulk is investigated, revealing a clear higher surface hardness than bulk for magnesium alloys, whereas lower surface hardness than bulk for aluminium alloys; for metals and oxides, the behavior varied. The deviation from the case of Young’s modulus being equal to reduced modulus is analyzed, for all three categories of materials, along with pile-up/sink in deformation mechanism. Evidence of indentation size effect is found and quantified for all three categories of materials.

1 Introduction

Nanoindentation provides load-depth curves for a monotonically increasing load, leading to the precise determination of different properties such as yield strength, hardness, elastic modulus, wear characteristics, etc. The usefulness of

E. P. Koumoulos · D. A. Dragatogiannis · C. A. Charitidis (✉)
School of Chemical Engineering, National Technical University of Athens, 9, Heroon
Polytechniou St., Zografos, 15780 Athens, Greece
e-mail: charitidis@chemeng.ntua.gr

nanoindentation to obtain the fundamental mechanical properties of materials has been widely demonstrated previously (e.g.). The nanoindentation test can provide information about the mechanical behaviour of the material when it is being deformed at the sub-micron scale. With the development of nanoindenters displacement discontinuities or discrete bursts (pop-in, pop-out and elbow phenomena) have been observed. These are characteristic of energy-absorbing or energy releasing events, occurring beneath the indenter tip.

The onset of plasticity in crystals is demonstrated by discrete bursts in the load-displacement curves, which are attributed to the initial nucleation of individual lattice dislocations (Gerberich et al. 1996). For such small indentations the crystal volume probed is typically so small as to be dislocation free. Thus indentation size effects at the nanometer scale are associated with the crystal being dislocation starved and requiring the nucleation of dislocations to initiate plasticity (Nix et al. 2007; Kelchner et al. 1998; Li et al. 2002). However, the pop-in may be associated with fracture of a surface oxide layer on some materials or may be connected with phase transformations widely reported in nanoindentation experiments of Si and ceramics (Schuh 2006; Venkataraman et al. 1992). Nevertheless, pop-in event is not a prerequisite condition for a permanent plastic deformation, since as reported during nanoindentation experiments many load curves show no excursion but did show plastic deformation. Also, plastic deformation behavior (residual impression 4 nm) was observed at indentation depth that was below the critical depth conducive to the pop-in event, which indicates that some dislocations were generated even before the pop-in event (Navamathavan et al. 2008). The first pop-in separates the region of fully elastic behavior, at lower loads from the region of elasto-plastic behavior at higher loads (Rabkin et al. 2010). When the first pop-in occurs, the maximum shear stress in the specimen is in the range of $G/30$ – $G/5$ (G -shear modulus), which is very close to the theoretical strength (Ogata et al. 2004). Pop-in loads vary over a wide range, and theoretical predictions based on a stress-assisted, thermally-activated, homogeneous-dislocation-nucleation model agree well with the experimentally measured statistical values (Chiu and Ngan 2002; Schuh and Lund 2004; Bei et al. 2008; Vliet et al. 2003; Schuh et al. 2005; Mason et al. 2006).

The strength of metals, oxides and alloys is strongly influenced by grain size (Kumar et al. 2003; Gleiter 2000). Materials in the nanocrystalline regime are characterized by superior yield and fracture strength, improved wear resistance, superplasticity observed at relatively low temperatures and high strain rates as compared with their microcrystalline counterparts (Masumura et al. 1998). According to the classical Hall–Petch law the yield or flow stress required for continuous plastic deformation increased with decreasing grain size. This phenomenon which observed for conventional grain size materials (1–100 μm diameter) is reversed in nanoscale since the yield stress decreased with decreasing grain size, below a critical grain size ($d \approx 10$ nm) for a variety of metals and alloys (Aifantis and Konstantinidis 2009). In fact, microstructures resulting in high long-life fatigue resistance will generally yield lower thresholds for fatigue crack growth, especially in ultra-fine and nanocrystalline regimes (Cavaliere 2009). Although mechanical properties of metals and oxides differ markedly in the bulk, they have an intriguingly similar response

to nanoindentations. Into nanoindentation regime, oxides, under certain conditions show a ductile response such as metals (Navarro et al. 2008). The onset of plasticity of engineering materials has been systematically investigated by means of two complementary techniques: macroscopic tensile or compression tests and depth-sensing nanoindentation. The scope of this research effort is to gain insight into the deformation mechanisms involved in local plasticity during nanoindentation of metals, oxides and alloys through mechanism investigation and correlation of ideal elastic modulus, hardness and Poisson ratio using nanoindentation data.

2 Experimental Details

2.1 Materials

The materials used in this work were selected on the basis of representing each main category of materials, i.e. metals (namely Cu, Co, Al, Ni, Pb and Si), aluminum (namely AA2024, AA5083, AA6082 and AA7075) and magnesium (namely AZ31, ZK10 and ZK30) alloys and oxides (namely Al₂O₃, TiO₂, SiO₂, Co₃O₄ and NiO).

2.2 Instrumentation: Approach

Nanoindentation testing was performed with Hysitron TriboLab[®] Nanomechanical Test Instrument, which allows the application of loads from 1 to 30,000.00 μ N and records the displacement as a function of applied loads with a high load resolution (1 nN) and a high displacement resolution (0.04 nm). The TriboLab[®] employed in this study is equipped with a scanning probe microscope (SPM), in which a sharp probe tip moves in a raster scan pattern across a sample surface using a three-axis piezo positioner. In all nanoindentation tests a total of 10 indents are averaged to determine the mean hardness (H) and elastic modulus (E) values for statistical purposes, with a spacing of 50 μ m, in a clean area environment with 45 % humidity and 23 °C ambient temperature. In order to operate under closed loop load or displacement control, feedback control option was used. All nanoindentation measurements have been performed with the standard three-sided pyramidal Berkovich probe, with an average radius of curvature of about 100 nm (Charitidis 2010).

Based on the half-space elastic deformation theory, H and E values can be extracted from the experimental data (load displacement curves) using the Oliver-Pharr (O&P) method (Cheng et al. 2002), where derived expressions for calculating the elastic modulus from indentation experiments are based on Sneddon's elastic contact theory (Eq. 1) (Sneddon 1948).

$$E_r = \frac{S\sqrt{\pi}}{2\beta\sqrt{A_c}} \quad (1)$$

where S is the unloading stiffness [initial slope of the unloading load-displacement curve at the maximum depth of penetration (or peak load)], A is the projected contact area between the tip and the substrate and β is a constant that depends on the geometry of the indenter [$\beta = 1.167$ for Berkovich tip (Oliver and Pharr 1992)]. Conventional nanoindentation hardness refers to the mean contact pressure; this hardness, which is the contact hardness H_c is actually dependent upon the geometry of the indenter (Eqs. 2–4).

$$H_c = \frac{F}{A} \quad (2)$$

where,

$$A(h_c) = 24,5h^2 + a_1h + a_{1/2}h^{1/2} + \dots + a_{1/16}h^{1/16} \quad (3)$$

and

$$h_c = h_m - \varepsilon \frac{P_m}{S_m} \quad (4)$$

where h_m is the total penetration depth of the indenter at peak load, P_m is the peak load at the indenter displacement depth h_m , and ε is an indenter geometry constant, equal to 0.75 for Berkovich indenter. Prior to indentation, the area function of the indenter tip was calibrated in a fused silica, a standard material for this purpose (Bei et al. 2005).

Plasticity is quantified based in the relation $\frac{W_{tot}-W_u}{W_{tot}}$ (where W_{tot} is the work of total indentation process and W_u is the work during unloading). It has recently established an approximately linear correlation ($\frac{H}{E^*} = k \frac{W_u}{W_{tot}}$ where k is a function of θ) between $\frac{W_{tot}-W_u}{W_{tot}}$ and $\frac{H}{E^*}$, first for a given indenter geometry (i.e. $\theta=90^\circ$) and later for conical indenters of a range of angles $60^\circ < \theta < 80^\circ$ (Cheng et al. 2002). From this relationship, the ratio $\frac{H}{E^*}$ can be obtained readily by integrating the loading–unloading curves to obtain $\frac{W_u}{W_{tot}}$. The ratio $\frac{H}{E^*}$ is of significant interest in tribology. This ratio multiplied by a geometric factor is the “plasticity index” that describes the deformation properties of a rough surface in contact with a smooth surface (Williams 1994). When the plasticity index is much less than unity, the deformation of asperities is likely to be entirely elastic.

3 Results and Discussion

3.1 Input Functions, Load–Displacement Curves

The relation (input function) of displacement change to time for the materials examined in this work is plotted in Fig. 1 (schematic trapezoidal load-time $P = P(t)$ input function). The loading–unloading curves of the probed materials (representative) are presented in Fig. 2 (comparison of probed materials is presented, for applied load of 5,000 μN); pure Ni exhibits higher resistance to applied

Fig. 1 Schematic trapezoidal of load-time $P = P(t)$ function for nanoindentation experiment

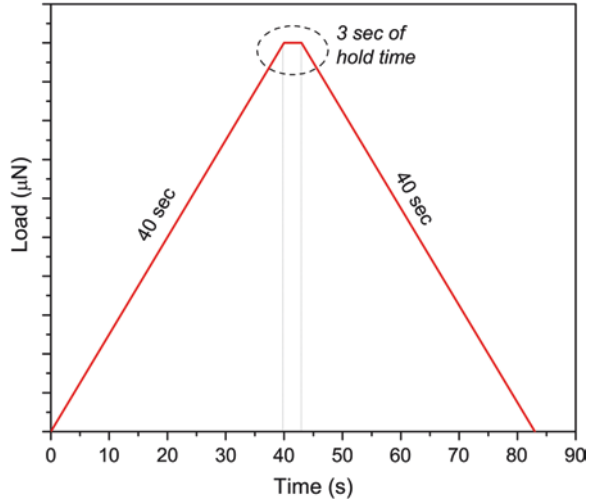
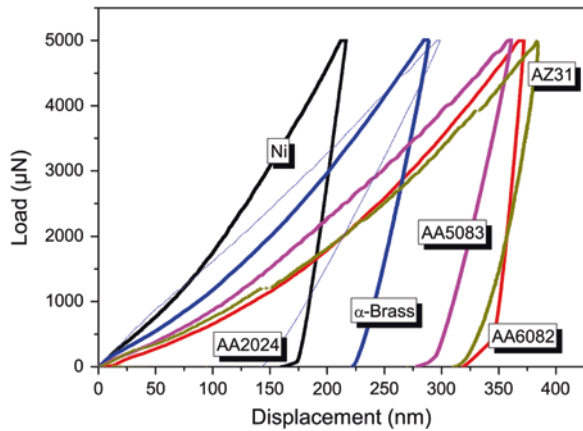


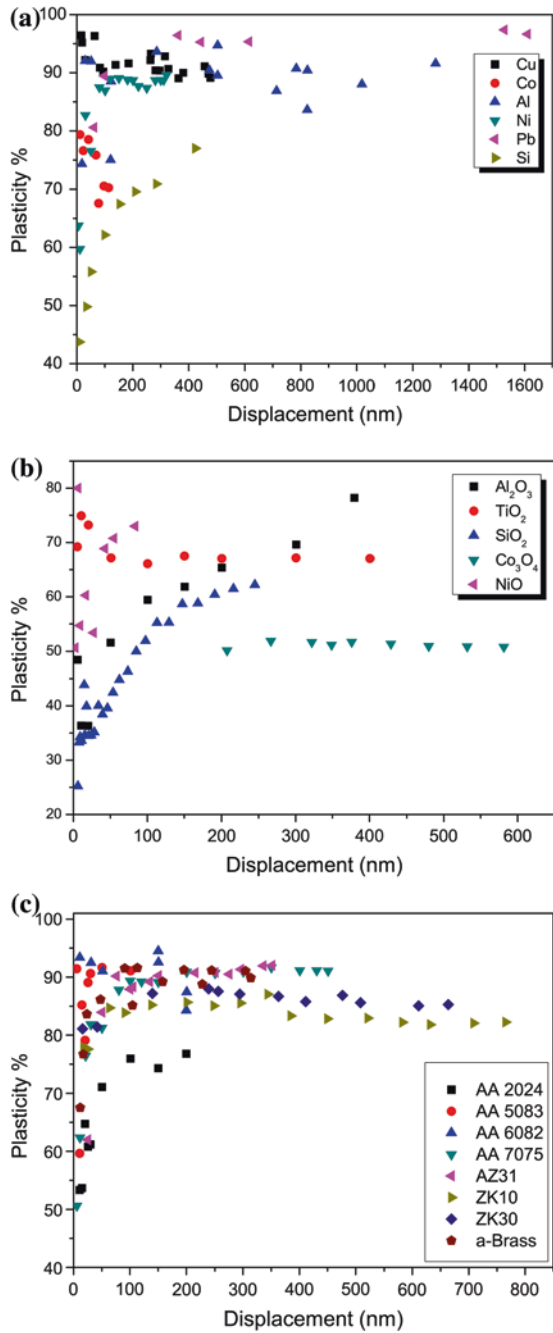
Fig. 2 Representative loading–unloading curves of metals and alloys for applied load of 5,000 µN



load (higher applied load values were needed for Ni to reach the same displacement of the rest of the materials). In the case of AA6082-T6, greater plasticity is revealed, i.e. energy stored at the material after the indentation is over (total integration of curve area), with AA2024 exhibiting higher elastic recovery (Fig. 3), in case of 5,000 µN of applied load.

In Fig. 3, the comparison of plastic deformation of metals reveals a low plasticity at low loads for the metalloid Si, implying enhancement of elasticity for weaker loads, while Cu, Al and Pb being the most plastic. This phenomenon at low loads may be attributed to the real physical effect of superelastic behavior of materials under microNewton scale forces, due to the inactivation of dislocations. It may also be an artifact due to the piling-up of the surface during indentation. Pile-up is the tendency of softer materials to overflow plastically out of the indented region

Fig. 3 Plasticity of (a) metals, (b) oxides and (c) alloys



(further analysis below); this phenomenon is connected to the material, which is really soft, and also to the geometry of the tip (decreasing the corner angle of the tip increases the plastic deformation of the material and thus its pile-up) and it leads to an overestimation of H and E (underestimation of the contact area). In oxides, Co_3O_4 exhibits a more stable plastic deformation across various displacements (~50 %), while Al_2O_3 ends up (at greater displacements) with the highest plastic deformation. Brass, aluminum and magnesium alloys exhibit an almost similar behaviour in plastic deformation, with AA2024 being more elastic at greater displacements.

3.2 SPM Imaging, Nanomechanical Properties

In Fig. 4, SPM imaging ($10 \times 10 \mu\text{m}$) of all samples is presented.

At each imposed depth E and H can be deduced from the curves. The graphs in Figs. 5, 6, 7 show the mean value of the H measurements as a function of the imposed displacement. As the indentation depth decreases below 100 nm, a rapid increase of the H value is observed. This rapid increase is probably a combination of either the real effect of a native oxide at the surface or an effect of the polishing procedure, or an artefact of the shape of the indenter tip for shallow displacements (Bei et al. 2005; Charitidis et al. 2012; Sangwal 2000). The high hydrostatic pressure exerted by the surrounding material allows plastic deformation at room temperature when conventional mechanical testing only leads to fracture. At low loads one phenomenon is very much prominent which is called Indentation Size Effect (ISE) due to imperfection in tip geometry. In several studies of materials ISE is revealed, which shows an increase in hardness with decreasing applied load. In a few cases, the hardness has been observed to decrease with decreasing indentation depth—the reverse ISE (Sangwal 2000). Apparently, the existence of ISE may hamper the accurate measurement of hardness value, and is attributed to experimental artifact, a consequence of inadequate measurement capability or presence of oxides on the surface. Other explanations include indenter-specimen

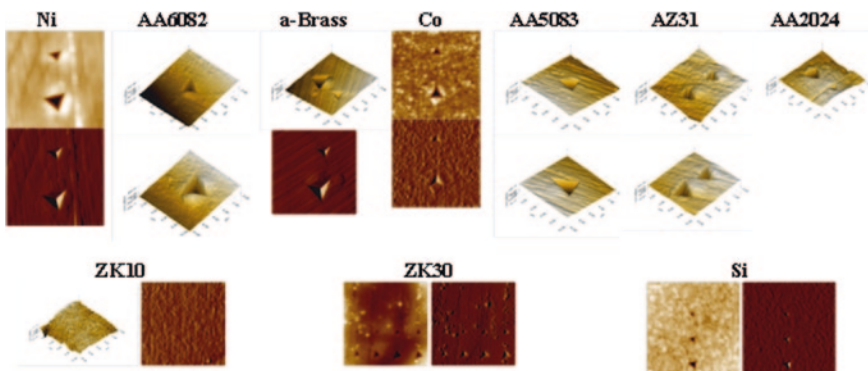


Fig. 4 Pile-up of final imprints through SPM imaging

Fig. 5 Hardness of metals for various displacements

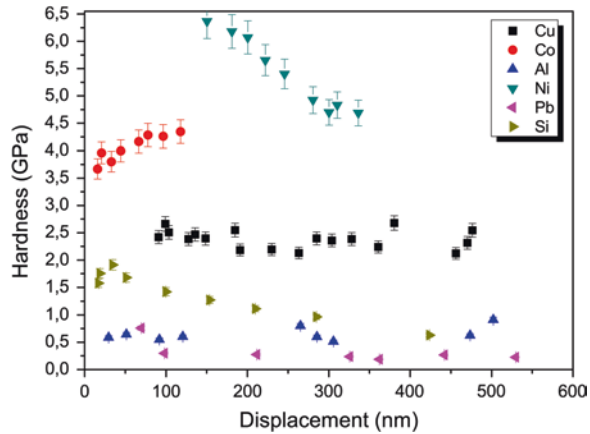
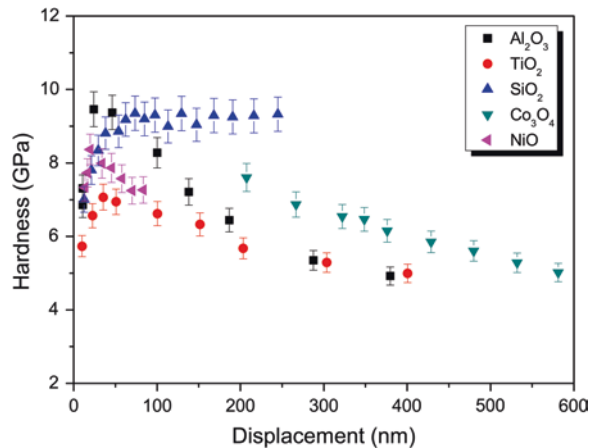


Fig. 6 Hardness of oxides for various displacements



friction, and changing dislocation density for shallow indents due to the presence, for instance, of geometrically necessary dislocations. Most of the dislocations stay generally confined around the residual imprint in a dense structure with many dislocation interactions (Charitidis et al. 2012). The reverse ISE phenomenon essentially takes place in crystals which readily undergo plastic deformation. The reverse ISE can be caused by: (1) the relative predominance of nucleation and multiplication of dislocations and (2) the relative predominance of the activity of either two sets of slip planes of a particular slip system or two slip systems below and above a particular load (Sangwal 2000).

Göken et al. proposed a method correcting pile-up effects and possible surface roughness (Göken et al. 2001). This method allows determining a correction factor for H based on the relation between the indentation modulus and Young's modulus, where Vlassak and Nix reported that E is highly dependent on the crystallographic orientation but that H is not (Vlassak and Nix 1994).

Fig. 7 Hardness of alloys for various displacements

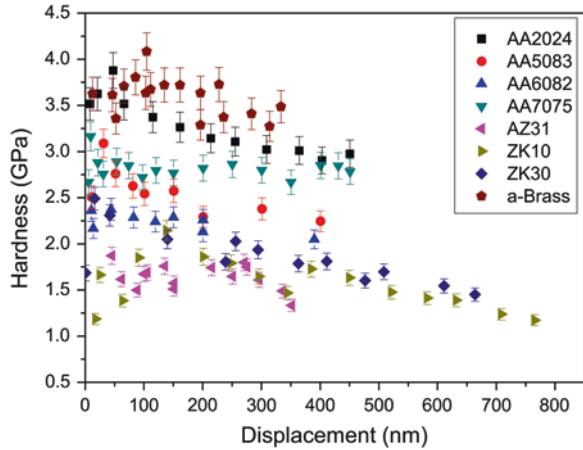
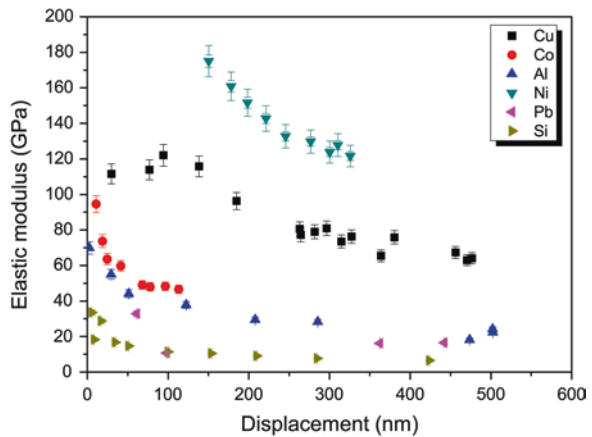


Fig. 8 Elastic modulus of metals for various displacements



Kese and Li proposed a method for accounting for the pile-up by considering the added pile-up contact area as semi-ellipses around Berkovich triangular impression (Kese and Li 2006), performed with post AFM scanning of the indented surface and measurement of the pile-up contact width for each of the three possible pile-up lobes. Lee et al. proposed a different approach by measuring the modulus of the material from early Hertzian loading analysis and using it to predict the pile-up (Lee et al. 2007). Some recent works in this field have reported study of pile-up around spherical indenters spherical-conical indenters, (Taljat and Pharr 2000; Maneiro and Rodriguez 2005) and also the effect of pile-up on thin film system measurements (Zhou et al. 2003).

In Figs. 8, 9, 10, the mean value of the elastic modulus is plotted versus the depth of the indentation. For aluminum alloys, an almost constant value for E (E_b for constant values over displacement) is obtained over the different applied test conditions, which seems reasonable. A range of values of ~50–100 GPa is

Fig. 9 Elastic modulus of oxides for various displacements

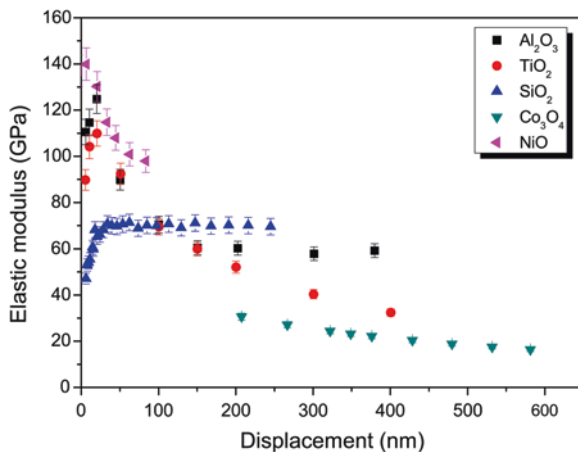
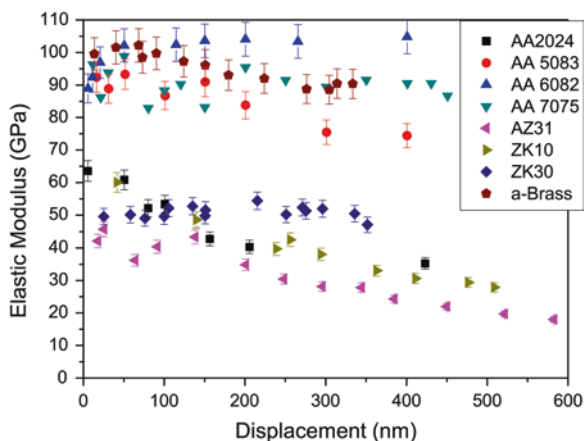
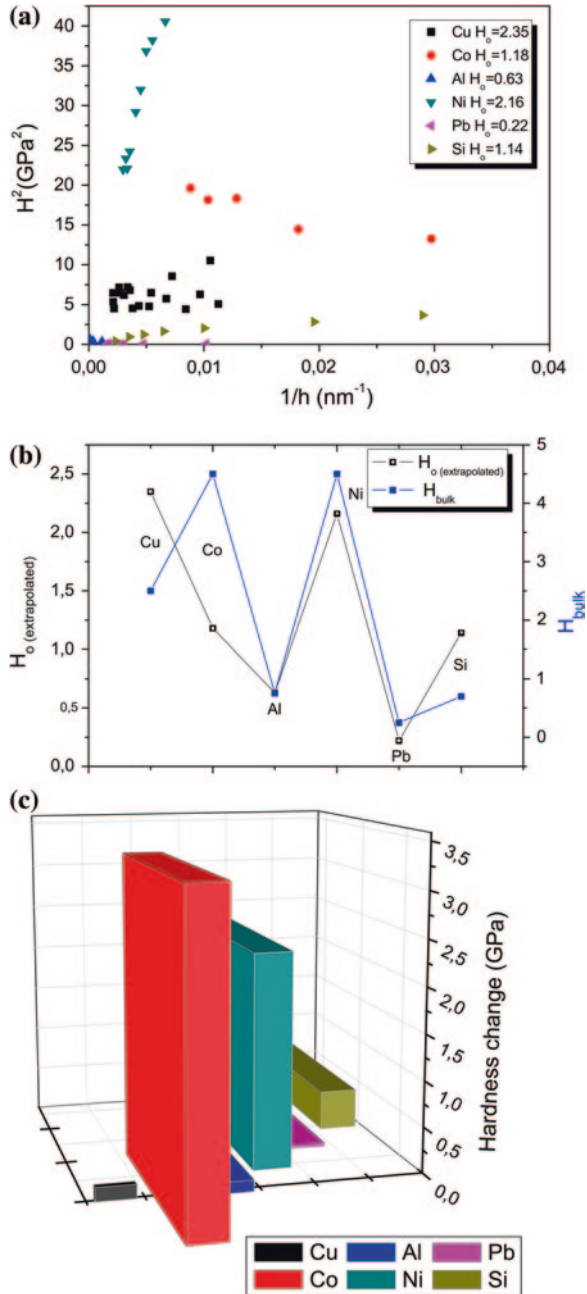


Fig. 10 Elastic modulus of alloys for various displacements



obtained which is in fairly good agreement with the reported Young’s modulus in literature (Calister 1990). The same is true for brass that leads to a value of ~100 GPa, relatively close to the 110 GPa reported (Sevillano et al. 2000). The deviation from these standard values is attributed to the elastic modulus values which are calculated by using the contact area from the indentation displacement considered since the first contact point with the initial flat surface, as described by the Oliver and Pharr method (1992). However, the plastically deformed zone around the indented area can pile-up against the indenter or sink-in, depending on the material’s work hardening. The consequence of this behaviour is a slight deviation from the standard values of the elastic modulus (Rodriguez and Gutierrez 2003). For brass, Vlassak and Nix determine 25 % of scatter between indentation modulus determined for different crystallographic orientations, but even higher discrepancies can be found, depending on the material (Vlassak and Nix 1994).

Fig. 11 **a** Square of the nanohardness value against the inverse of the depth. **b** Comparison of hardness at bulk and extrapolated hardness. **c** Hardness change of metals



In Figs. 11, 12, 13a, the square of the nanohardness value obtained in the indentation tests is plotted as a function of the reciprocal of the indentation depth. It can be seen that a linear relation is closely followed for the most of the

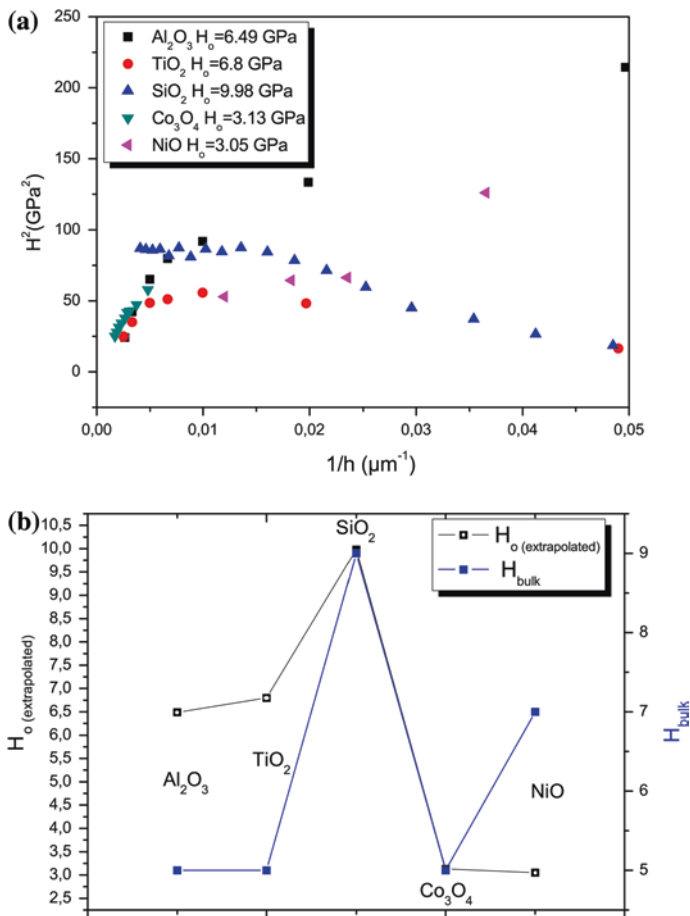
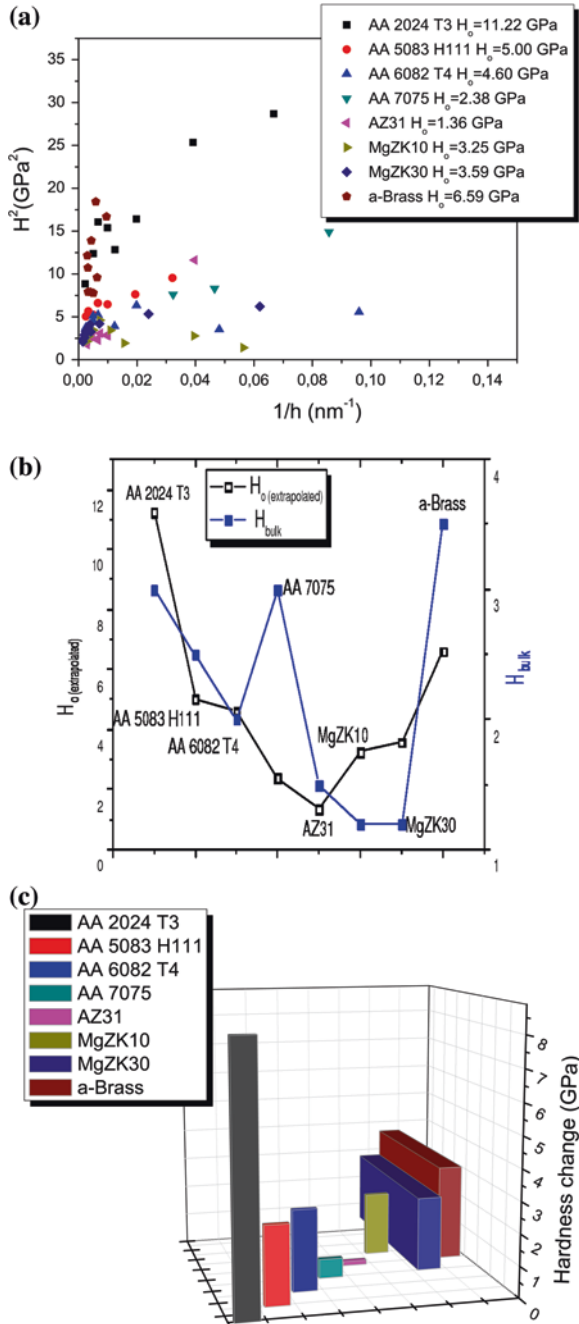


Fig. 12 **a** Square of the nanohardness value against the inverse of the depth. **b** Comparison of hardness at bulk and extrapolated hardness. **c** Hardness change of oxides

materials, in agreement with literature (Schwaiger et al. 2003). The value of the hardness at infinite depth, H_0 , can be estimated by extrapolating the mentioned linear relations to $\frac{1}{h} = 0$. In the literature, however, it is reported that nanoindentation hardness data do not follow this linear trend over the whole measurement range (Lim and Chaudhri 1999; Swadener et al. 2002), an evident phenomenon observed also in this work. Instead, at small indentation depths they start to deviate from the predicted linear curve. The obtained values for hardness at infinite depth are shown in the table embedded in Fig. 13a. The comparison of H_0 and mean H at surface region (0–400 nm) (H_s) is presented in Figs. 11, 12, 13b–c, where hardness at infinite displacement clearly matches with H_s for AA6082-T6, brass and AA5083-H111. However, comparison of both hardness values of e.g. pure Ni and AA2024 exhibit great deviation (reduced plastic deformation in higher applied loads, dominated by sink-in), revealing that in order to reach constant

Fig. 13 **a** Square of the nanoindentation hardness value against the inverse of the depth. **b** Comparison of hardness at bulk and extrapolated hardness. **c** Hardness change of alloys



nanomechanical properties (of bulk material), indenting in greater displacement is needed.

Although mechanical properties of metals, alloys and oxides differ markedly in the bulk, they have an intriguingly similar response to nanoindentations. When

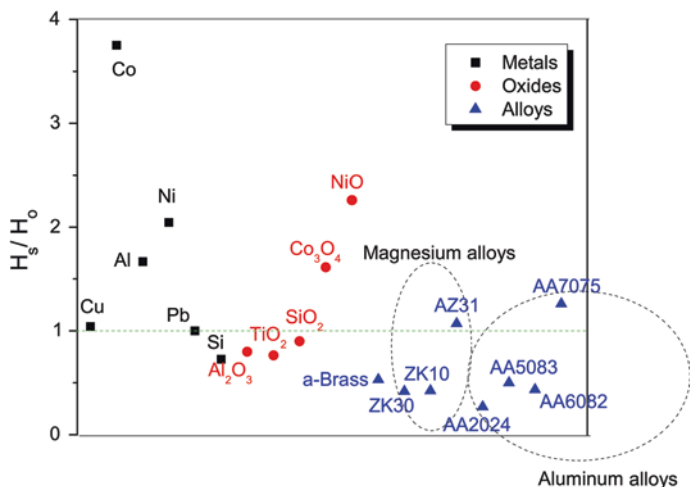


Fig. 14 H_{bulk}/H_0 ratio for all categories

scaling down into the nanoindentation regime, e.g. oxides, which in the bulk are known to be brittle, under certain conditions show a ductile response in which the nucleation of cracks is averted (Rhee et al. 2001). Some of these surfaces can even transit between as the external load increases, so does the average pressure. Once the resolved shear stress attains a certain threshold value the crystal yields and dislocation loops are generated. Then, the pressure is partially released and a low-energy-barrier dislocation loop source begins to operate. Comparing metals and oxides, we remark that in the nanoindentation region, the ratio between the respective hardnesses $\frac{H_{\text{oxide}}}{H_{\text{metal}}}$ varies (Navarro et al. 2008) (Fig. 14).

We turn now to the different behaviours of the three categories of materials using the ratio q between their hardness's in the surface region and in the bulk (i.e. extrapolated hardness at infinite displacement), i.e. $q = \frac{H_s}{H_0}$. During the nanoindentation process of metals, alloys and oxides surface the effective volume that is probed is small enough to avoid encompassing any pre-existing dislocations. Under these conditions, following the nucleation of the first yield point, the hardness in the region of constant low hardness corresponds to the operation of a low-barrier dislocation source. In the case of $q > 1$, as the tip excursion progresses into the bulk, pre-existing dislocations able to glide start being activated. The hardness is now controlled, Taylor-type, by the work hardening related to the dislocation density. As is well known, this results in a rather low value of H_0 , smaller than the one corresponding to the operation of the loop source, and one ends up with a value of $q \gg 1$. On the other hand, the case of $q < 1$ is probably attributed to the fact that in the bulk, pre-existing dislocations are pinned and stresses cannot make them glide. The reason why low-barrier dislocation sources, similar to the ones proposed to control hardness in the low effective volume limit, do not seem to operate in the bulk is not yet clear. The following explanation may exist; dislocations introduced by the source can interact with pre-existing pinned dislocations -or even among themselves-resulting

in very immobile locks, which further impede the motion of subsequently nucleated dislocations. If the effective volume is small, no pre-existing dislocations exist in it and the locking does not take place (Navarro et al. 2008).

3.3 Pop-ins-Power Law

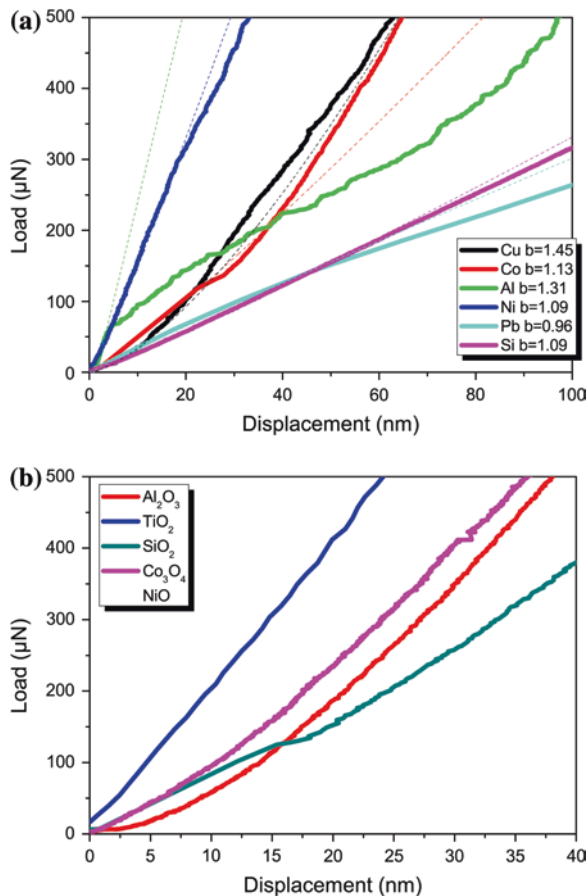
Figure 15 shows that the loading–unloading curves for all samples, exhibit interesting local discontinuities measured in the load-controlled test of this work; these are characteristic of energy-absorbing or energy-releasing events occurring beneath the indenter tip. Three different physical phenomena usually occur in nanoindentation testing of metals of various states of bonding and structural order; dislocation activity during a shallow indentation, shear localization into ‘shear bands’, and phase transformation with a significant volume increase during unloading of indentation (Schuh 2006).

Many materials undergo phase transformations when subjected to large hydrostatic stresses, and the pressure beneath a nanoindenter is generally quite high (on the order of several GPa) (Schuh 2006). Association of pop-in events with the beginning of material phase transformation is simple a revelation of sudden extrusion of highly plastic transformed material from underneath the indenter. The sudden displacement discontinuities, i.e. the pop-ins, were observed in the loading part. The first pop-in (referred as yield type pop-in in literature) implies that strain is accommodated by an abrupt existence of atomic activity beneath the indenter, that could be attributed to activation of a dislocation source (Schuh 2006).

Small displacements are equivalent to a linear-elastic response; the curvature of the free energy diagram at an equilibrium position gives rise to a particular elastic constant, represented by the initial slope in a force distance diagram. Larger displacements elicit a non-linear response. However, one property of particular interest is the theoretical shear strength of the material: the limit where a further increase in displacements elicits no further increase in the restoring force. The general relationship between the applied load (P) and the penetration depth (h) of an indenter may be described by power law as $P = ah^b$ where the constants a and b are geometric and material parameters, respectively (Charitidis 2010).

Load-unload curves often reveal discontinuities or pop-ins in the loading part. Various examples are reported in the literature for metals, although a complete explanation of this behaviour has been under investigation (Schuh et al. 2005). While yield points reported for Si and some other ceramics may be connected to phase transformations [when the mean contact pressure of hardness indentations closely matches the critical pressure a possible structural transformation is triggered (Schuh 2006; Johnson 1970)], the exhibited yield points in most of the known metals clearly reveal the beginning of dislocation plasticity (the plastic deformation of metals occurs by the motion of dislocations). Evaluations of the maximum stress under the tip reveal that stress values (almost equal to theoretical shear stress) occur in the surface of the metal (dislocation activity starts first at

Fig. 15 Hertzian elastic fit to representative indentations on metals and alloys

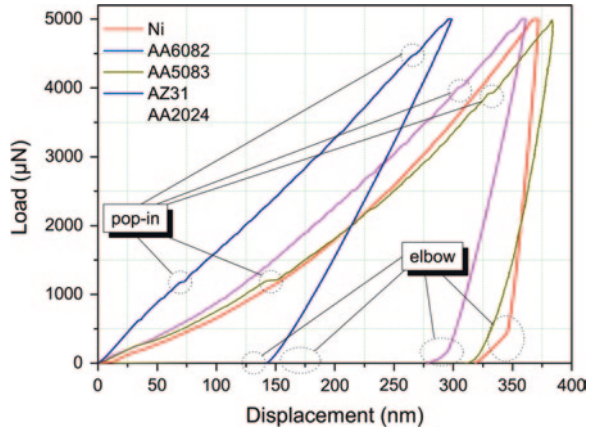


the yield type pop-in load), as generation of dislocations in the nano-scale stressed volume from the perfect crystal environment (Wo and Ngan 2005).

As shown in Fig. 15, the transition from purely elastic to elastic/plastic deformation i.e. gradual slope change (yield-type 'pop-in') of all materials occurs in the load–displacement curves, at approximately 10–30 nm. The onset-stress for plastic deformation of fcc single crystals of pure metals is very low and their flow stress exhibits an extraordinary high hardening capacity. The dislocation structure developed in a single crystal depends significantly on the applied strain and the path the straining is accomplished. It usually starts by the formation of micro and macro slip bands and proceeds by the generation of cells and cell block structures. Further deforming, keeps the process of fragmentation on. Finally, at very large strains a saturation structure with a minimum crystallite size is reached. For copper single crystals deformed at room temperature, this crystallite size is in the order of a few 100 nm.

The indenter displacement in most of the cases is accommodated plastically, and only a small portion is elastically recovered on unloading. Discontinuity in load

Fig. 16 Pop-ins and elbows indicated in nanoindentation loading–unloading curves



displacement, which is commonly referred as ‘pop-in’ effect (Fig. 16), was observed frequently in aluminum, indicating a process of producing mobile dislocations. The initial pop-in is usually associated with homogeneous dislocation nucleation, while subsequent similar events often involve avalanches of dislocation activity (Wo and Ngan 2005). In addition to defects, there may be residual stresses in the surface which influence the occurrence of the initial discontinuities in the load–displacement curve (Charitidis et al. 2012). Additionally, roughness such as surface steps could act as stress concentrators or alternatively exhibit a long-range effect of the order of several contact radius (Zimmerman et al. 2001). Gogotsi et al. (2000), Domnich and Gogotsi (2002) and Juliano et al. (2003) proposed that the “pop-out” behavior corresponds to the formation of metastable Si-XII/Si-III crystalline phases, in case of silicon nanoindentation. High stresses can cause plastic deformation not only by dislocation activity, but also by pressure-induced phase transformations to denser crystalline and amorphous forms (Ge et al. 2004). The transformation mechanisms are dependent on the indentation testing conditions e.g. peak load and loading/unloading rate or indenter angle (Jang et al. 2005). This results in a change in the unloading curve either as a “pop-out” or elbow phenomenon (Fig. 16), which indicates a lower contact depth, h_c , and therefore may influence the calculation of hardness. Thus, the experimental measurement of the hardness of indented materials is slightly higher than that of the ideal value.

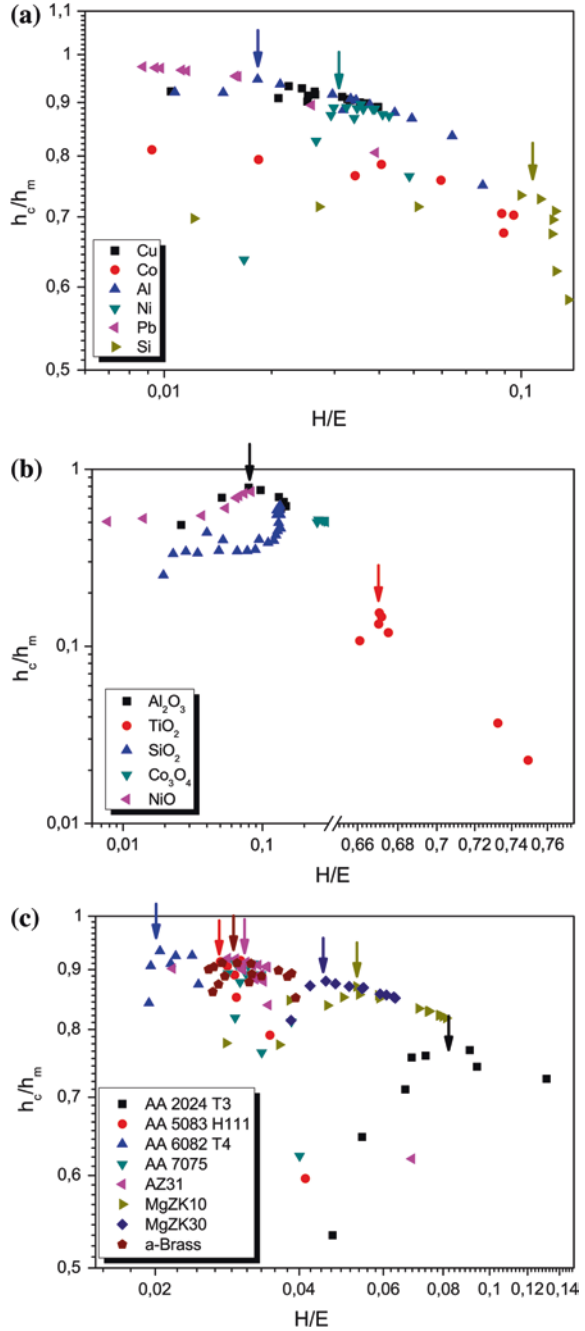
3.4 Pile-up/Sink-in Deformation

The contact area is influenced by the formation of pile-ups and sink-ins during the indentation process. To accurately measure the indentation contact area, pile-ups/sink-ins should be appropriately accounted for. The presence of creep (time/rate dependent property of materials) during nanoindentation has an effect on pile-up, which results in incorrect measurement of the material properties. Fischer-Cripps

observed this behaviour in aluminum where the measured elastic modulus was much less than expected (Fischer-Cripps 2004). Rar et al. observed that the same material when allowed to creep for a long duration produced a higher value of pile-up/sink-in indicating a switch from an initial elastic sink-into a plastic pile-up (Rar et al. 2005). Significant pile-up forms for materials start from an $\frac{h_c}{h_m}$ value of 0.7–0.88 (Khan et al. 2010).

In Fig. 17a–c, the normalized pile-up/sink-in height $\frac{h_c}{h_m}$ is plotted versus the normalized hardness $\frac{H}{E}$ for all samples. It is reported that materials with high $\frac{H}{E}$, i.e. hard materials, undergo sink-in whereas materials pile-up for low $\frac{H}{E}$, i.e. soft materials. In general it is also observed that in the case when $\frac{H}{E}$ is high (hard materials), materials undergo sink-ins regardless of work hardening and strain rate sensitivity and all materials collapse to a single curve. In addition, for materials with low $\frac{H}{E}$, soft materials, pile-up depends on the degree of work hardening (Charitidis et al. 2012). Softer materials, i.e., low $\frac{H}{E}$, possess a plastic zone, which is hemispherical in shape and meet the surface well outside the radius of the circle of contact and pile-up is expected. On the other hand, for materials with high values of $\frac{H}{E}$, i.e. harder materials, the plastic zone is contained within the boundary of the circle of contact and the elastic deformations that accommodate the volume of indentation are spread at a greater distance from the indenter. Higher stresses are expected in high $\frac{H}{E}$, hard materials, and high stress concentrations develop towards the indenter tip, whereas in case of low $\frac{H}{E}$, soft materials, the stresses are lower and are distributed more evenly across the cross-section of the material (Charitidis et al. 2012). Rate sensitive materials experience less pile-up compared to rate insensitive materials due strain hardening. Cheng and Cheng reported a 22 % pile-up for a work hardening exponent (Cheng and Cheng 1998). This is consistent with the fact that when $\frac{h_c}{h_m}$ approaches 1 for small $\frac{H}{E}$, deformation is intimately dominated by pile-up (Hill et al. 1989). On the other hand when $\frac{h_c}{h_m}$ approaches 0 for large $\frac{H}{E}$ it corresponds to purely elastic deformation and is apparently dominated by sink-in in a manner prescribed by Hertzian contact mechanics (Hertz 1986). The dependence on the elastic–plastic behaviour of the material is related to the response of the material being indented (Hertz 1986). The degree of sink-in or pile-up of the materials is reported to be expressed as a function of the work hardening exponent (Norbury and Samuel 1928). During nanoindentation, materials with a low work hardening exponent accommodate the volume of material ejecting it to the sides of the tip (pile-up). In the same way, in materials with a high value of n ($n > 0.3$) the sink-in effect is revealed. In both cases, the contact area is different from the cross-sectional area estimated by the method described by Oliver and Pharr (1992). Consequently, there is a deviation between the real and the computed area that is controlled by the elastic–plastic behavior.

Fig. 17 Normalised pile-up/sink-in height h_c/h_m of metals, oxides and alloys versus H/E ratio



3.5 Poisson Ratio and Modulus Correlation

Elastic properties of materials are usually characterized by Young's modulus, shear modulus, bulk modulus and Poisson's ratio. For isotropic materials only two of these elastic constants are independent and other constants are calculated by using the relations given by the theory of elasticity. The best choice for these two independent moduli is considered as the shear modulus (G) and the bulk modulus (B) (Ledbetter 1977). The shear modulus relates to strain response of a body to shear or torsional stress. It involves change of shape without change of volume. On the other hand, the B describes the strain response of a body to hydrostatic stress involving change in volume without change of shape. However, the best-known elastic constant is E , which is most commonly used in engineering design (Phani and Sanyal 2008).

Materials with different Poisson's ratios behave very differently mechanically. Properties range from 'rubbery' to 'dilatational', between which are 'stiff' materials like metals and minerals, 'compliant' materials like polymers and 'spongy' materials like foams. The physical significance of ν is revealed by various interrelations between theoretical elastic properties (90). At different temperatures and pressures, crystalline materials can undergo phase transitions and, attracting considerable debate, so too can glasses and liquids (Bridgman 1949; Greaves et al. 2008; Poole 1997). For ceramics, glasses and semiconductors (Zhang et al. 1985; Perottoni and Jornada 2002), $\frac{B}{G} \approx \frac{5}{3}$ and $\nu \rightarrow \frac{1}{4}$. Likewise, metals are stiff (Cottrell 1990; Kelly et al. 1967), $\frac{B}{G}$ ranging from 1.7 to 5.6 and ν from 0.25 to 0.42 (Kelly et al. 1967). In sharp contrast, polymers are compliant and yet they share similar values (Lakes and Wineman 2006; Lu et al. 1997): that is, $\frac{B}{G} \approx \frac{8}{3}$ and $\nu \approx 0.33$, the difference relating to the magnitude of the elastic module, decades smaller than for inorganic materials. Poisson's ratio can be followed through abrupt changes in mechanical properties. For example, when metals melt, ν increases from ~ 0.3 to 0.5 (Santamaria et al. 2009; Jensen et al. 2010). During the collapse of microporous crystals, ν rises from directionally auxetic values to isotropic values of 0.2 typical of many glasses (Valle et al. 2008; Grima et al. 2000). With densification Poisson's ratio for glasses continues to rise, for silica increasing from 0.19 to 0.33 (Zha et al. 1994). Poisson's ratio is intimately connected with the way structural elements are packed. For gold or platinum-based bulk metallic glasses, for example, which represent some of the densest metals because of the variety of atom sizes, $\nu \rightarrow \frac{1}{2}$. Crystalline metals are less densely packed, typified by hard metals like steel for which $\nu \approx \frac{1}{3}$. By contrast, the density of covalent solids is less and so is Poisson's ratio (Greaves et al. 2011).

Through contact analysis, Eq. 5 is derived:

$$\frac{1}{E^*} = \frac{1 - \nu_i^2}{E_i} + \frac{1 - \nu_s^2}{E_s} \quad (5)$$

where E^* is the reduced modulus, E_i is the Young's modulus of the indenter, ν_i is the Poisson ratio of the indenter, E_s is the Young's modulus of the sample and ν_s is the Poisson ratio of the sample.

Fig. 18 Deviation from $E^* = E_s$ (red dashed line) for (a) metals, (b) oxides and (c) alloys through nanoindentation

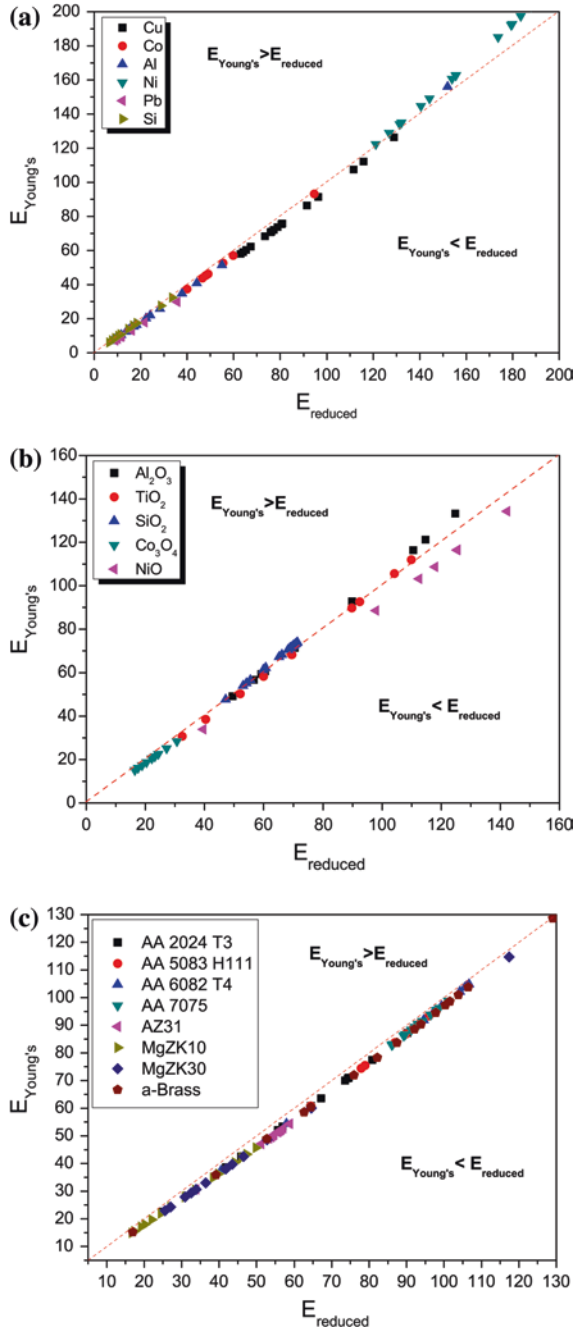


Fig. 19 Young’s modulus correlation with Poisson ratio, following obtained values

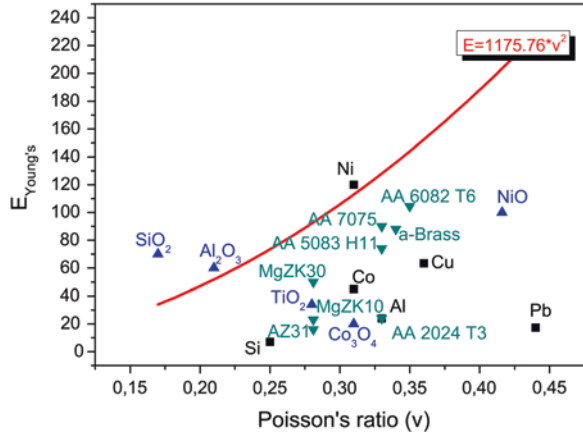
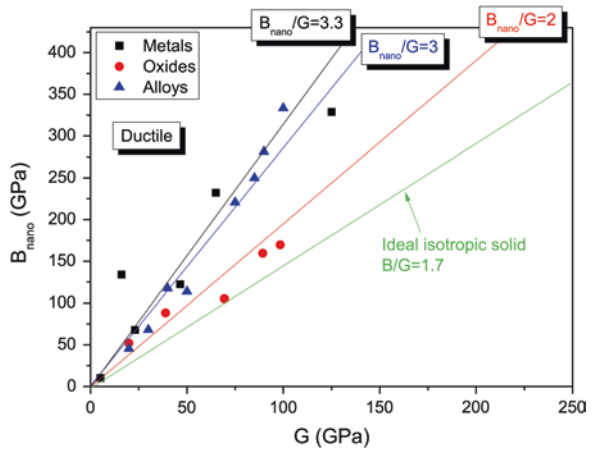


Fig. 20 Plot of bulk modulus versus shear modulus for metals, oxides and alloys through nanoindentation



Analytically, when the so-called reduced modulus is equal to Young’s modulus ($E^* = E_s$), (Fig. 18) is assumed, then using Eqs. 5 and 6 are derived (for $E_i = 1140$ GPa and $\nu_i = 0.07$ of diamond indenter): (Fig. 19)

$$E_s = \frac{\nu_s^2}{1 - \nu_i^2} E_i = 1175.76 \nu_s^2 \tag{6}$$

Figure 20 shows the variation of bulk moduli of three categories of samples with Young’s moduli. Bulk modulus values (B_{nano} in Table 1) were estimated from nanoindentation Young’s moduli values using Eq. (7) (Barrett et al. 1973):

$$E = 3 * B_{nano} (1 - 2\nu) \tag{7}$$

where E is Young’s modulus, B_{nano} is bulk modulus, and ν is Poisson’s ratio.

Table 1 Mechanical properties and Poisson ratio of studied materials

		E_b (GPa)	H_s (GPa)	G (GPa)	E_b/G	H_s/E_b	H_o (GPa)	$q (H_s/H_o) \nu$	B_{nano} (GPa)	
Metals	Cu	65	2.5	44.7	1.45414	0.03846	2.4	1.04167	0.36	232
	Co	46.5	4.5	75	0.62	0.09677	1.2	3.75	0.31	122
	Al	23.06	1	26	0.88692	0.04337	0.6	1.66667	0.33	67
	Ni	125	4.5	76	1.64474	0.036	2.2	2.04545	0.31	328
	Pb	16.07	0.2	13.1	1.22672	0.01245	0.2	1	0.44	133
	Si	5.125	0.8	50.9	0.10069	0.1561	1.1	0.72727	0.25	10
Alloys	a-Brass	90	3.5	40	2.25	0.03889	6.6	0.5303	0.34	281
	ZK30	50	1.5	17	2.94118	0.03	3.6	0.41667	0.28	113
	ZK10	30	1.4	17	1.76471	0.04667	3.3	0.42424	0.28	68
	AZ31	20	1.5	17	1.17647	0.075	1.4	1.07143	0.28	45
	AA2024	40	3	27	1.48148	0.075	11.2	0.26786	0.33	117
	AA5083	75	2.5	28	2.67857	0.03333	5	0.5	0.33	220
	AA6082	100	2	27	3.7037	0.02	4.6	0.43478	0.35	333
	AA7075	85	3	27	3.14815	0.03529	2.38	1.2605	0.33	250
Metal oxides	Al ₂ O ₃	89.37	5.2	18	4.965	0.05819	6.5	0.8	0.22	159
	TiO ₂	38.87	5.2	90	0.43189	0.13378	6.8	0.76471	0.28	88
	SiO ₂	69.41	9	31	2.23903	0.12966	10	0.9	0.17	105
	Co ₃ O ₄	19.83	5	83.71	0.23689	0.25214	3.1	1.6129	0.31	52
	NiO	98.46	7	–	–	0.07109	3.1	2.25806	0.21	169

Ductility and brittleness relate to the extreme response of materials strained outside their elastic limits, so any relationship with ν would seem at first non-intuitive. However, Poisson’s ratio measures the resistance of a material to volume change (B —Bulk modulus) balanced against the resistance to shape change (G —shear modulus). Occurring within the elastic regime, any links with properties beyond the yield point must necessarily involve the time-dependent processes of densification and/or flow, already discussed for glasses above. Just as viscoelastic behaviour is expressed in terms of time-dependent bulk and shear modulus, with Poisson’s ratio $\nu(t)$ gradually changing between elastic values, we might expect the starting value of ν to provide a metric for anticipating mechanical changes, not just in glasses but also in crystalline materials, resulting in ductility (starting from a high ν) or embrittlement (starting from a low ν). At either extreme the microstructure will play a part, whether through cracks, dislocations, shear bands, impurities, inclusions or other means (Xi et al. 2005). Although there is no simple link between interatomic potentials and mechanical toughness in polycrystalline materials, Poisson’s ratio ν has proved valuable for many years as a criterion for the brittle-ductile transition exhibited by metals (Cottrell 1990; Jiang et al. 2010). The old proposal that grains in polycrystalline materials might be cemented together by a thin layer of amorphous material “analogous to the condition of a greatly under cooled liquid” has often been challenged (Rosenhain et al. 1913). However, recent atomistic simulations of crystalline grains and grain boundaries seem to confirm the dynamic consequences of this idea in many details (Zhang et al. 2009). The strengths of pure metals at low

temperatures are known to be mainly governed by the strengths of grain boundaries (Cottrell 1990). These usually exceed the crystalline cleavage strength, which is governed by the dynamics of dislocations generated at the crack tip (Kelly et al. 1967). This would suggest that soft metals like gold, silver or copper might be ductile because they originate from melts that are fragile.

Conversely, hard metals such as tungsten, iridium or chromium might be brittle because, as melts, they are stronger. If this were the case then there would be consequences for the density fluctuations frozen into the grain boundaries, which will be weaker for soft metals than for brittle metals. By the same token, grain boundaries would be more ergodic in soft compared with brittle metals.

3.6 Indentation Size Effect and Onset of Plasticity

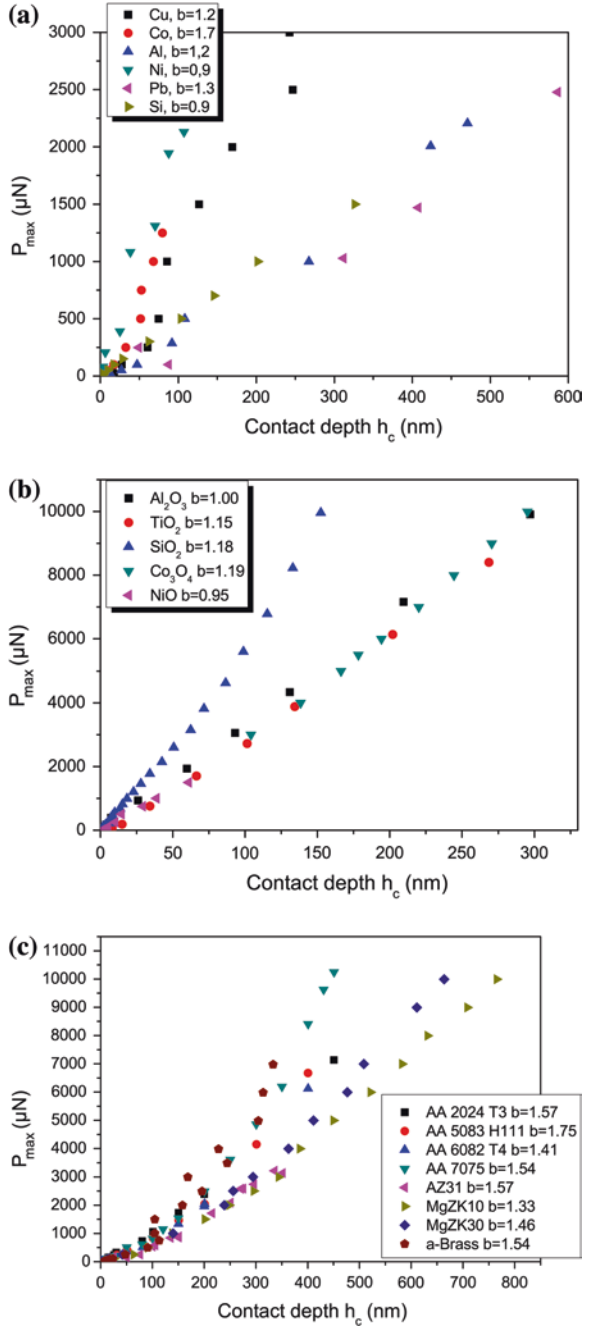
Due to the very low contact area between the indenter and the sample, very high stresses can be developed. The high hydrostatic pressure exerted by the surrounding material allows plastic deformation at room temperature when conventional mechanical testing only leads to fracture. It is revealed that some materials exhibit ISE, which shows an increase in hardness with decreasing applied load (Samuels 1989). Apparently, the existence of ISE may hamper the accurate measurement of hardness value, and is attributed to experimental artifact, a consequence of inadequate measurement capability or presence of oxides on the surface (Li et al. 1993). Other explanations include indenter-specimen friction (Li et al. 1993), and changing dislocation density for shallow indents due to the presence, for instance, of geometrically necessary dislocations (Gaillard et al. 2006).

The Berkovich indenter generates dislocations organized in a quite complex way during a nanoindentation test, even for very low deformations (Leipner et al. 2001), making difficult the formulation for the stress field generated, even during an elastic deformation, as well as its modelling. Most of the dislocations stay generally confined around the residual imprint in a dense structure with many dislocation interactions (Tromas and Gaillard 2004).

Firstly, we used the empirical equation for describing the ISE in the Meyer's law (Kolemen 2006; Sahin et al. 2007), which uses a correlation technique between the applied indentation test load and the resultant indentation size using a simple power law, $P_{max} = Ch_c^n$, where C and n are constants derived directly from curve fitting of the experimental data. In particular, the constant C is a measure of materials resistant to plastic deformation and the exponent n , sometimes referred to as the Meyer index, is usually considered as a measure of ISE. Compared to the definition of the apparent hardness, no ISE would be observed for $n = 2$ (Peng et al. 2004).

The nanoindentation data for the material examined in the present study was plotted in Fig. 21. The data showed power law relationship, implying that the traditional Meyer's law was suitable for describing the nanoindentation data. The calculated n values pointed out higher apparent nanohardness values at lower loads, in other words, the presence of an ISE. In the bulk, hardness in the plastic stage, measured by micro indentations involving large effective volumes, is commonly interpreted in

Fig. 21 Nanoindentation applied load plotted contact depth for (a) metals, (b) oxides and (c) alloys



terms of a Nix and Gao mechanism (Nix and Gao 1998). This mechanism, based on the pioneering ideas of Taylor (Cottrell 1953), explains the value of hardness in terms of the work hardening of the material due to a mixture of pre-existing and

geometrically necessary dislocations (GNDs). Often, this leads to the so-called indentation size effect, by which hardness increases at low penetration depths. Evidence of this ISE has been found both in oxides and metals (Peng et al. 2004). In the case of metals, even probing deep in the bulk (no ISE), the values of H are larger than the macroscopic yield strength of bulk as hardness in the plastic region is controlled by work hardening. In the case of oxides, values of yield strength of bulk are not easily found as many micro indentation studies do not intend to resolve either the elastic region or the yield point, and directly probe the plastic region. Nevertheless, some of the existing values show that H values are on the order of yield strength of bulk.

4 Concluding Remarks

Although Hertzian elastic contact theory is commonly used for the evaluation of initial load–displacement curves, it may not be an adequate model for all materials. Pure Ni exhibits higher resistance to applied load (higher applied load values were needed for Ni to reach the same displacement of the rest of the materials). All examined materials, exhibited interesting local discontinuities measured in the load-controlled test, which are characteristic of energy-absorbing or energy-releasing events occurring beneath the indenter tip. In the load–displacement curves, brass exhibited earlier transition from purely elastic to elastic/plastic deformation i.e. gradual slope change (yield-type ‘pop-in’), followed by pure Ni (AZ31 and aluminum alloys exhibited late transition). Aluminum alloys (AA5083 and AA6082) exhibited significant elbow effect in unloading part. Hardness at ~400 nm displacement and extrapolated hardness show almost same behaviour for examined metals and alloys (in agreement with similar studies in literature). Comparison of both hardness values of pure Ni and AA2024 exhibit great deviation (reduced plastic deformation in higher applied loads, dominated by sink-in), revealing that in order to reach constant nano mechanical properties (of bulk material), indenting in greater displacement is needed. Additionally it has to be considered, that in case the imprint size is significantly larger than the dimension of the deformation-controlling microstructure, the hardness should be independent of the imprint size. The ratio of surface hardness to hardness in bulk was investigated, revealing a clear higher surface hardness than bulk for magnesium alloys, whereas lower surface hardness than bulk for aluminum alloys; for metals and oxides, the behaviour varied. Furthermore, the deviation from the case of Young’s modulus being equal to reduced modulus was also studied, for all three categories of materials, along with pile-up/sink in deformation mechanism. Evidence of Indentation Size Effect (ISE) has been found both in oxides and metals. In the case of metals, even probing deep in the bulk (no ISE), the values of H are larger than the macroscopic yield strength of bulk as hardness in the plastic region is controlled by work hardening. In the case of oxides, values of yield strength of bulk are not easily found as many microindentation studies do not intend to

resolve either the elastic region or the yield point, and directly probe the plastic region.

Acknowledgments This work was partially supported by the EU FP7 Project “Micro and Nanocrystalline Functionally Graded Materials for Transport Applications” (MATTRANS) under Grant Agreement no. 228869 and partially supported by NTUA funded project for basic research PEVE-NTUA-2010/65187900.

References

- Aifantis KE, Konstantinidis AA (2009) Hall-Petch revisited at the nanoscale. *Mater Sci Eng, B* 163:139–144
- Barrett CR, Nix WD, Tetelman AS (1973) The principles of engineering materials. Printice-Hall Incorporation, New Jersey
- Bei H, George EP, Hay JL, Pharr GM (2005) Influence of indenter tip geometry on elastic deformation during nanoindentation. *Phys Rev Lett* 95(045501):1–4
- Bei H, Gao YF, Shim S, George EP, Pharr GM (2008) Strength differences arising from homogeneous versus heterogeneous dislocation nucleation. *Phys Rev B* 77(6060103):1–4
- Bridgman PW (1949) The physics of high pressure. Bell, London
- Callister WD (1990) Materials science and engineering. Wiley, New York
- Cavaliere P (2009) Fatigue properties and crack behavior of ultra-fine and nanocrystalline pure metals. *Int J Fatigue* 31(10):1476–1489
- Charitidis CA (2010) Nanomechanical and nanotribological properties of carbon-based thin films: A review. *Int J Refract Metal Hard Mater* 28(1):51–70
- Charitidis CA, Dragatogiannis DA, Koumoulos EP, Kartsonakis IA (2012) Residual stress and deformation mechanism of friction stir welded aluminum alloys by nanoindentation. *Mater Sci Eng, A* 540:226–234
- Cheng YT, Cheng CM (1998) Relationships between hardness, elastic modulus, and the work of indentation. *Appl Phys Lett* 73(5):614–616
- Cheng YT, Li Z, Cheng CM (2002) Scaling relationships for indentation measurements. *Philos Mag A* 82(10):1822–1829
- Chiu YL, Ngan AHW (2002) Time-dependent characteristics of incipient plasticity in nanoindentation of a Ni3Al single crystal. *Acta Mater* 50(6):1599–1611
- Cottrell AH (1953) Dislocations and plastic flow in crystals. Clarendon, Oxford
- Cottrell AH (1990) Advances in physical metallurgy, In: Charles JA, Smith GC (eds) Institute of metals, London
- Domnich V, Gogotsi Y (2002) Phase transformations in silicon under contact loading. *Rev Adv Mater Sci* 3:1–36
- Fischer-Cripps AC (2004) A simple phenomenological approach to nanoindentation creep. *Mater Sci Eng A* 385(1–2):74–82
- Gaillard Y, Tromas C, Woïrgard J (2006) Quantitative analysis of dislocation pile-ups nucleated during nanoindentation in MgO. *Acta Mater* 54:1409–1417
- Ge D, Domnich V, Juliano T, Stach EA, Gogotsi Y (2004) Structural damage in boron carbide under contact loading. *Acta Mater* 52:3921–3927
- Gerberich WW, Nelson JC, Lilleodden ET, Anderson P, Wyrobek JT (1996) Indentation induced dislocation nucleation: the initial yield point. *Acta Mater* 44(9):3585–3598
- Gleiter H (2000) Nanostructured materials: basic concepts and microstructure. *Acta Mater* 48(1):1–29
- Gogotsi YG, Domnich V, Dub SN, Kailer A, Nickel KG (2000) Cyclic nanoindentation and raman microspectroscopy study of phase transformations in semiconductor. *J Mater Res* 15:871–879

- Göken M, Kempf M, Nix WD (2001) Hardness and modulus of the lamellar microstructure in PST-TiAl studied by nanoindentations and AFM. *Acta Mater* 49(5):901–903
- Greaves GN, Meneau F, Kargl F, Ward D, Holliman P, Albergamo F (2007) Zeolite collapse and polymorphism. *J Phys: Condens Matt* 19(41):415102 1–17
- Greaves GN, Wilding MC, Fearn S, Langstaff D, Kargl F, Cox S, Van QV, Majérus O, Benmore CJ, Weber R, Martin CM, Hennet L (2008) Detection of first-order liquid/liquid phase transitions in yttrium oxide-aluminum oxide melts. *Science* 322:566–570
- Greaves GN, Greer AL, Lakes RS, Rouxel T (2011) Poisson's ratio and modern materials. *Nat Mater* 10:823–837
- Grima JN, Jackson R, Alderson A, Evans KE (2000) Do Zeolites have negative poisson's ratios. *Adv Mater B* 12(24):1912–1917
- Hertz H (1986) *Miscellaneous papers*. Macmillan, London
- Hill R, Storåkers B, Zdunek AB (1989) A theoretical study of the brinell hardness test. *Proc Royal Soc London A* 423(1865):301–330
- Jang JI, Lance MJ, Wen SQ, Tsui TY, Pharr GM (2005) Indentation-induced phase transformations in silicon: influences of load, rate and indenter angle on the transformation behaviour. *Acta Mater* 53(6):1759–1770
- Jensen BJ, Cherne FJ, Cooley JC, Zhernokletov MV, Kovalev AE (2010) Shock melting of cerium. *Phys Rev B* 81(21):214109 1–8
- Jiang MQ, Dai LH (2010) Short-range-order effects on intrinsic plasticity of metallic glasses. *Philos Mag Lett* 90(4):269–277
- Johnson KL (1970) The correlation of indentation experiments. *J Mech Phys Solids* 18:115–126
- Juliano T, Gogotsi Y, Domnich V (2003) Effect of indentation unloading conditions on phase transformation induced events in silicon. *J Mater Res* 18(05):1192–1201
- Kelchner CL, Plimpton SJ, Hamilton JC (1998) Dislocation nucleation and defect structure during surface indentation. *Phys Rev B* 58(17):11085–11088
- Kelly A, Tyson WR, Cottrell AH (1967) Ductile and brittle crystals. *Phil Mag* 15:567–586
- Kese K, Li ZC (2006) Semi-ellipse method for accounting for the pile-up contact area during nanoindentation with the Berkovich indenter. *Scripta Mater* 55:699–702
- Khan MK, Hainsworth SV, Fitzpatrick ME, Edwards L (2010) A combined experimental and finite element approach for determining mechanical properties of aluminium alloys by nanoindentation. *Comput Mater Sci* 49:4751–4760
- Kolemen U (2006) Analysis of ISE in micro hardness measurements of bulk MgB₂ superconductors using different models. *J Alloy Compd* 425:429–435
- Kumar KS, Swygenhoven HV, Suresh S (2003) Mechanical behaviour of nanocrystalline metals and alloys. *Acta Mater* 51(19):5743–5774
- Lakes RS, Wineman A (2006) On Poisson's ratio in linearly viscoelastic solids. *J Elast* 85(1):45–63
- Ledbetter HM (1977) Ratio of the shear and Young's moduli for polycrystalline metallic elements. *Mater Sci Eng* 27(2):133–135
- Lee YH, Baek U, Kim YI, Nahm SH (2007) On the measurement of pile-up corrected hardness based on the early Hertzian loading analysis. *Mater Lett* 61(19–20):4039–4042
- Leipner HS, Lorenz D, Zecker A, Lei H, Grau P (2001) Nanoindentation pop-in effect in semiconductors. *Phys B* 308–310:446–449
- Li H, Ghosh A, Han YH, Bradt RC (1993) The Frictional Component of the Indentation Size Effect in Low Hardness Testing. *Journal of Materials Research* 8(5):1028–1032
- Li J, Vliet KJV, Zhu T, Yip S, Suresh S (2002) Atomistic mechanisms governing elastic limit and incipient plasticity in crystals. *Nature* 418:307–310
- Lim YY, Chaudhri MM (1999) The effect of the indenter load on the nano hardness of ductile metals: an experimental study on polycrystalline work-hardened and annealed oxygen-free copper. *Philos Mag A* 79:2979–3000
- Loerting T, Giovambattista N (2006) Amorphous ices: experiments and numerical simulations. *J Phys Condens Matt* 18: R919–R977

- Lu H, Zhang X, Krauss WG (1997) Uniaxial, shear, and Poisson relaxation and their conversion to bulk relaxation: studies on poly (methyl methacrylate). *Polym Eng Sci* 37:1053–1064
- Maneiro MAG, Rodriguez J (2005) Pile up effect on nanoindentation tests with spherical-conical tips. *Scripta Mater* 52:593–598
- Mason JK, Lund AC, Schuh CA (2006) Determining the activation energy and volume for the onset of plasticity during nanoindentation. *Phys Rev B* 73(054102):1–15
- Masumura RA, Hazzledine PM, Pande CS (1998) Yield stress of fine grained materials. *Acta Mater* 46(13):4527–4534
- Navamathavan R, Park SJ, Hahn JH, Choi CK (2008) Nanoindentation ‘pop-in’ phenomenon in epitaxial ZnO thin films on sapphire substrates. *Mater Charact* 59:359–364
- Navarro V, de la Fuente OR, Mascaraque A, Rojo JM (2008) Plastic properties of gold surfaces nanopatterned by ion beam sputtering. *Phys Rev Lett B* 78(224023):1–14
- Nix WD, Gao H (1998) Indentation size effects in crystalline materials: a law for strain gradient plasticity. *J Mech Phys Solids* 46(3):411–425
- Nix WD, Greer JR, Feng G, Lilleodden ET (2007) Deformation at the nanometer and micrometer length scales: effects of strain gradients and dislocation starvation. *Thin Solid Films* 515(6):3152–3157
- Norbury AL, Samuel T (1928) The recovery and sinking-in or piling-up of material in the brinell test, and the effects of these factors on the correlation of the brinell with certain other hardness tests. *J Iron Steel Ind* 117:673–687
- Ogata S, Li J, Hirotsaki N, Shibutani Y, Yip S (2004) Ideal shear strain of metals and ceramics. *Phys Rev B* 70:104104
- Oliver WC, Pharr GM (1992) An improved technique for determining hardness and elastic modulus using load and displacement sensing indentation experiments. *J Mater Res* 7:1564–1583
- Peng Z, Gong J, Miao H (2004) On the description of indentation size effect in hardness testing for ceramics: Analysis of the nanoindentation data. *J Eur Ceram Soc* 24:2193–2201
- Perotoni CA, Jornada JA (2002) First-principles calculation of the structure and elastic properties of a 3D-polymerized fullerite. *Phys Rev B* 65(224208):1–6
- Phani KK, Sanyal D (2008) The relations between the shear modulus, the bulk modulus and Young’s modulus for porous isotropic ceramic materials. *Mat Sci Eng, A* 490(1–2):305–312
- Poole PH, Grande T, Angell CA, McMillan PE (1997) Polymorphism in liquids and glasses. *Science* 275:322–323
- Rabkin E, Deuschle JK, Baretzky B (2010) On the nature of displacement bursts during nanoindentation of ultrathin Ni films on sapphire. *Acta Mater* 58:1589–1598
- Rar A, Sohn S, Oliver WC, Goldsby DL, Tullis TE, Pharr GM (2005) On the measurement of creep by nanoindentation with continuous stiffness techniques. In: Abstracts of symposium on fundamentals of nanoindentation and nanotribology III, Boston, Massachusetts, U.S.A November 29–December 3
- Rhee YW, Kim HW, Deng Y, Lawn BR (2001) Brittle fracture versus quasiplasticity in ceramics: a simple predictive index. *J Am Ceramic Soc* 84:561–565
- Rodriguez R, Gutierrez I (2003) Correlation between nanoindentation and tensile properties: influence of the indentation size effect. *Mater Sci Eng, A* 361(1–2):377–384
- Rosenhain W, Ewen D (1913) The intercrystalline cohesion of metals. *J Inst Metals* 10:119–148
- Sahin O, Uzun O, Kolemen U, Ucar N (2007) Mechanical characterization for β -Sn single crystals using nanoindentation tests. *Mater Charact* 59(4):427–434
- Samuels LE (1989) ASTM STP 889, American society for testing and materials, Philadelphia, 1986, p 5
- Sangwal K (2000) On the reverse indentation size effect and micro hardness measurement of solids. *Mater Chem Phys* 63:145–152
- Santamaria-Perez D, Ross M, Errandonea D, Mukherjee GD, Mezouar M, Boehler R (2009) X-ray diffraction measurements of Mo melting to 119 GPa and the high pressure phase diagram. *J Chem Phys* 130(124509):1–8
- Schuh CA (2006) Nanoindentation studies of materials. *Mater Today* 9(5):32–39

- Schuh CA, Lund AC (2004) Application of nucleation theory to the rate dependence of incipient plasticity during nanoindentation. *J Mater Res* 19(07):2152–2158
- Schuh CA, Mason JK, Lund AC (2005) Quantitative insight into dislocation nucleation from high-temperature nanoindentation experiments. *Nat Mater* 4(8):617–621
- Schwaiger R, Moser B, Dao M, Chollacoop N, Suresh S (2003) Some critical experiments on the strain-rate sensitivity of nanocrystalline nickel. *Acta Mater* 51(17):5159–5172
- Sevillano JG, Buessler P, Vrieze J, Kaluza W, Bouaziz O, Jung T, Bonifaz E, Meizoso AM, Martinez Esnaola JM, Ocaña I (2000) ECSC Steel RTD Final report, CECA7210-PR-044
- Sneddon IN (1948) Boussinesq's problem for a rigid cone. *Math Proc Cambridge* 44:492–507
- Swadener JG, George EP, Pharr GM (2002) The correlation of the indentation size effect measured with indenters of various shapes. *J Mech Phys Solids* 50(4):681–694
- Taljat B, Pharr GM (2000) Measurement of residual stresses by load and depth sensing spherical indentation. *Mater Res Symp Proc* 594:519–524
- Tomas C, Gaillard Y (2004) *Encyclopedia of materials science and technology*. Elsevier Science, Amsterdam
- Valle CS, Lethbridge ZAD, Sinogeikin SV, Williams JJ, Walton R I, Evans KE, Bass JD (2008) Negative Poisson's ratios in siliceous zeolite MFI-silicalite. *J Chem Phys* 128(18): 184503 1–5
- Venkataraman S, Kohlstedt DL, Gerberich WW (1992) Microscratch analysis of the work of adhesion for Pt thin films on NiO. *Mater Res* 7:1126–1132
- Vlassak JJ, Nix WD (1994) Measuring the elastic properties of anisotropic materials by means of indentation experiments. *J Mech Phys Solids* 42(8):1223–1245
- Vliet KJV, Li J, Zhu T, Yip S, Suresh S (2003) Quantifying the early stages of plasticity through nanoscale experiments and simulations. *Phys Rev B* 67(104105):1–15
- Williams JA (1994) *Engineering tribology*. Oxford University Press, Oxford
- Wo PC, Zuo L, Ngan AHW (2005) Time-dependent incipient plasticity in Ni₃Al as observed in nanoindentation. *J Mater Res* 20:489–495
- Xi XK, Zhao DQ, Pan MX, Wang WH, Wu Y, Lewandowski JJ (2005) Fracture of brittle metallic glasses: brittleness or plasticity. *Phys Rev Lett* 94(12):125510 1–4
- Zha CS, Hemley RJ, Mao HK, Duffy TS, Meade C (1994) Acoustic velocities and refractive index of SiO₂ glass to 57.5 GPa by Brillouin scattering. *Phys Rev B* 50:13105–13112
- Zhang SB, Cohen ML, Louie SG (1985) Interface potential changes and Schottky barriers. *Phys Rev B* 32(3955):3955–3957
- Zhang H, Srolovitz DJ, Douglas JF, Warren JA (2009) Grain boundaries exhibit the dynamics of glass-forming liquids. In: *Proceedings of the national academy science*, 106:7735–7740, USA
- Zhou XY, Jiang ZD, Wang HR, Yu RX (2003) Investigation on methods for dealing with pile-up errors in evaluating the mechanical properties of thin metal films at sub-micron scale on hard substrates by nanoindentation technique. *Mater Sci Eng, A* 488(1–2):318–322
- Zimmerman JA, Kelchner CL, Klein PA, Hamilton JC, Foiles SM (2001) Surface step effects on nanoindentation. *Phys Rev Lett* 87(16): 165507 1–4